Experimental and Theoretical Investigations on the Methyl−Methyl Recombination Reaction

Baoshan Wang,† Hua Hou,† Laurie M. Yoder, James T. Muckerman, and Christopher Fockenberg*

Chemistry Department 555A, Brookhaven National Laboratory, P.O. Box 5000, Upton, New York 11973-5000

Received: May 27, 2003

The temperature and pressure dependence of the rate constant of the methyl−methyl recombination reaction with He bath gas has been studied using time-resolved time-of-flight mass spectrometry. Methyl radicals were produced by the 193 nm laser photolysis of acetone. In the observed temperature (300−700 K) and pressure (0.6−10 Torr) range, the rate constant exhibits a negative temperature dependence and falloff behavior typical for recombination reactions. The integrity of the measurements has been validated by determining the recombination rate constant with Ar (1 Torr) as the bath gas at room temperature and by analyzing the yield of the reaction product, ethane. In addition, rate constants were calculated theoretically using variable reaction coordinate transition state theory in a manner that improves upon the previous treatment of Wagner and Wardlaw by incorporating high-level ab initio results. The calculated high-pressure rate constant can be expressed as $k_\infty^{\text{theory}}(T) = 7.42 \times 10^{-11}\ (T/298\ \text{K})^{-0.69}\ e^{-88\text{K}/T}$ cm^3 molecule^{-1} s^{-1}. With reasonable downward energy transfer parameters, the experimentally observed pressure dependence of the rate constants for Ar, He, and H_2 bath gases were reproduced very well using master equation analysis. Troe's equation, describing the *T* and *P* dependence of the recombination rate constant, was fit to a set of data for He as bath gas comprised of rate constants from this work and taken from the literature. With $k_\infty(T)$ set to be the high-pressure limit rate constant calculated here, the other remaining parameters can be given by $k_0(T) = 1.17 \times 10^{-25}\ (T/298\ \text{K})^{-3.75}\ e^{-494\ \text{K}/T}$ cm^6 molecule^{-2} s^{-1} and $F_{\text{cent}}(T) = e^{-T/570\text{K}}$.

Introduction

In addition to its considerable importance in combustion processes of hydrocarbon fuels, the methyl−methyl recombination reaction (R1) has been investigated in our laboratory as part of an effort to study radical−radical reaction kinetics involving the methyl radical as a reaction partner. Frequently, the methyl concentration is chosen in excess over the second radical species, so that the rate constant for R1, k_1, and its temperature and pressure dependence is crucial in the analysis of the experimental data

$$CH_3 + CH_3 + M \rightarrow C_2H_6 + M \qquad \text{(R1)}$$

R1 has been studied extensively both experimentally and theoretically covering wide temperature ($T = 200-1700$ K) and pressure ($P = 0.3-10^5$ Torr) ranges predominantly with Ar bath gas.[1−14] However, few studies have been done for R1 with He as a collision partner. Slagle et al. measured k_1 at 296, 577, and 810 K and 2.4−22.6 Torr using a tubular reactor coupled to a photoionization mass spectrometer.[2] At $T = 296$ K and pressures less than 10.5 Torr, the measured rate constants surprisingly did not show any pressure dependence, and an average value for k_1 of 3.7×10^{-11} cm^3 molecule^{-1} s^{-1} was reported. Only at higher temperatures, the rate constants showed a falloff behavior. Using the same experimental apparatus, Stoliarov et al. and Knyazev et al. recently measured k_1 ancillary to rate constants of reactions between methyl and a number of hydrocarbon radical species in a pressure range of 1−10 Torr.[15−17] Again, no pressure dependence was observed for the room-temperature rate constants at $P = 1-3.8$ Torr. However, the reported data have significant uncertainties, e.g., the room-temperature rate constants at 3.8 Torr vary from 3.7 to 4.7×10^{-11} cm^3 molecule^{-1} s^{-1}. Deters et al. measured a smaller value of 2.9×10^{-11} cm^3 molecule^{-1} s^{-1} at 298 K and 1 Torr using a flow-tube reactor with a microwave discharge and laser magnetic resonance as detection technique.[18] For the same experimental conditions, Cody et al. reported an even smaller rate constant of $(2.44 \pm 0.52) \times 10^{-11}$ cm^3 molecule^{-1} s^{-1}, using a discharge-flow reactor apparatus coupled to a quadrupole mass spectrometer.[19] The rate constant was found to be slightly dependent on the bath gas pressure (He) at the two pressures chosen (0.6 and 1 Torr). For higher pressures (7.6−678 Torr), De Avillez Pereira et al. measured k_1 at 290, 473, and 700 K using a laser flash photolysis/UV-absorption spectrometer.[20] Unfortunately, the lack of accurate temperature-dependent absorption cross sections for the CH_3 radical at 216.4 nm and nonnegligible secondary reactions introduced relatively large systematic errors in the results. By modeling the detailed reaction mechanism at 290 K, the authors noted that the experimental rate constants were overestimated by approximately 10−20%. An earlier measurement at 298 K and 100 Torr by Fahr et al. reported $k_1 = 5.2 \times 10^{-11}$ cm^3 molecule^{-1} s^{-1}.[21]

Hessler and Ogren performed a global fit to the experimental rate constants with Ar as bath gas using various empirical parametric equations.[14] Oref's J-equation[22,23] was demonstrated to have the best performance among the five equations

* To whom correspondence should be addressed. E-mail: fknberg@bnl.gov.

† Present address: College of Chemistry and Molecular Sciences, Wuhan University, Wuhan, 430072 P.R. China.

10.1021/jp030657h CCC: $25.00
Published on Web 12/03/2003

examined. The results reported are $k_\infty(T) = 8.78 \times 10^{-11}$ $e^{-T/723\ K}$ cm^3 molecule^{-1} s^{-1}, $k_0(T) = 9.04 \times 10^{-27}$ cm^6 molecule^{-2} s^{-1}, and $J(T) = (e^{T/268\ K} - 1)^2$. As the authors pointed out, fitting low- and/or high-pressure limit rate constants in isothermal data sets, which span only limited pressure ranges, can be highly uncertain. Also, the analytical expression used to describe the temperature dependence of, e.g., the fitted k_∞ is a function of the particular global model. Because almost all of the rate constants of the methyl−methyl recombination reaction reported in the literature or measured here lie in the falloff region, we decided to obtain $k_\infty(T)$ from fitting high-pressure limit rate constants calculated with an empirical model of this reaction based on work by Wardlaw and Marcus[9] and Wagner and Wardlaw[10] using flexible transition state theory.[24,25] Both of these calculations used an empirical potential energy surface and switching function (describing the evolution of the CH_3 geometry and conserved frequencies at the transition state), which was adjusted by Wagner and Wardlaw[10] to fit the experimental data of Slagle et al.[2] In contrast, the potential energy surface used in this work was built from high-level ab initio data describing the C−C potential and the barrier height of the hindered rotation. In addition, a new switching function was constructed from the C−C distance dependence of the CH_3 splay angle replacing the exponential function employed by Wagner and Wardlaw. A master equation analysis provided rate constants in the falloff region and allowed a comparison of the efficiency of collisional deactivation among the Ar, He, and H_2 bath gases used here. Good agreement between theory and experiments was found for the bath gases studied covering temperatures from 200 to 1350 K.

Methyl−methyl recombination reaction kinetics have also been studied computationally using various theoretical methods, including the statistical adiabatic channel model (SACM) and transition state theory (TST).[8−12]

Experimental Section

Measurements were carried out using laser photolysis and repetitively sampled time-of-flight mass spectrometry (TOFMS), which has been described in detail elsewhere.[26] Only an overview will be given below.

The reactor consists of a quartz tube ($d = 1$ cm, $l = 43$ cm) coated with a thin film of platinum on the outside, which was used to heat the tube electrically. The temperature of the reaction mixture during an experiment was continually monitored at six equally spaced locations along the reactor using six K-type thermocouples. The local deviation from the average temperature was less than 5%. The inner surface was coated with boric acid and heat treated at 700 K in a vacuum. Precursor molecules (acetone) mixed into bath gases (He, H_2, and Ar: Praxair, 99.999%) flowed at a constant velocity of 10 m/s through the tube. The gas flow and the precursor concentrations were set by mass-flow controllers (Tylan General, FC 260). A 0.5-mm diameter orifice in the wall of the reactor allowed the sampling of the gas mixtures in the tube, a fraction of which was subsequently photoionized by VUV radiation emitted from a hollow cathode lamp (McPherson model 630). The lamp was operated with either Ar ($h\nu = 11.62$ and 11.83 eV) or H_2 (many lines, with the main line at 10.2 eV) in the discharge at pressures of 200 mTorr for Ar and 400 mTorr for H_2. The radiation was coupled into the main chamber via a glass capillary in a windowless configuration, which allows the use of the whole emission spectrum of H_2 extending up to 14 eV with an overall intensity being at least 10 times higher compared to Ar. By a burst of rapid successive extractions of ions into the flight tube, a string of mass spectra was acquired covering 25 ms in intervals of 48 μs. For a typical experiment, tens of thousands of these data sets were summed to give an acceptable signal-to-noise ratio. Radicals were created in the photolysis of a suitable precursor species using the emission of an excimer laser, which was fired about 2 ms into the acquisition of a string of mass spectra. The delay was generated by a digital delay generator (Stanford Research Systems DG535). The laser pulse was observed with a photodiode, and its delay time with respect to the start of the acquisition of a set of mass spectra was monitored with a digital oscilloscope (LeCroy LT344).

Special effort was made to measure the initial methyl concentration, $[CH_3]_0$, which has to be known to good accuracy in order to determine the rate constants k_1 precisely. Methyl radicals were conveniently produced by the 193 nm laser (ArF, Lambda Physik COMPEX 205) photolysis of acetone. Acetone (Mallinckrodt, 99.7%) was purified by multiple freeze−pump−thaw cycles. The primary photolysis pathway is

$$CH_3C(O)CH_3 + h\nu\ (193\ nm) \rightarrow 2\ CH_3 + CO \quad (R2a)$$

with two minor channels leading to

$$\rightarrow CH_2CO + CH_4 \quad (R2b)$$

$$\rightarrow H + CH_3C(O)CH_2 \quad (R2c)$$

The yield of channel R2b has been measured in this laboratory to be (2.2 ± 0.5)% by comparing the signals from ketene and acetone.[27] This result is in good agreement with the upper limit of 2% reported by Lightfoot et al.[28] In addition, because we were neither able to detect hydrogen atoms nor distinguish acetonyl ($CH_3C(O)CH_2$) radicals (channel R2c) from cracking of acetone into the same channel, the yield of channel R2c was estimated alternatively from the signal at $m/e = 72$, which was attributed to methyl ethyl ketone produced in the reaction of acetonyl with methyl radicals. An upper limit of (0.5 ± 0.2)% was obtained, which is significantly smaller than the estimate of 3% reported by Lightfoot et al. However, this indirect result is subject to a large uncertainty as discussed earlier.[27]

Additionally, a small fraction of the methyl radicals was subsequently photolyzed by the same laser pulse producing methylene (CH_2) and hydrogen atoms[27,28]

$$CH_3 + h\nu\ (193\ nm) \rightarrow CH_2 + H \quad (R3)$$

Unfortunately, the CH_2 signal fell below the detection limit. However, it could be estimated from previous experiments that about 1−2% of the methyl radicals were photolyzed even at the low laser fluences used ($\leq$35 mJ/cm^2).[27] Therefore, 96% ($\approx$100% − 2.2% − 0.5% − 1.5%) was used as the best estimate for the overall yield of methyl radicals. The uncertainty is about ±4% including the possible errors in the yields of channels R2b, R2c, and R3. The absolute initial concentration of CH_3 was calculated as follows:

$$[CH_3]_0 = 2\frac{\Delta\{acetone^+\}}{\{acetone^+\}_0}[acetone]_0\ 96\% \quad (E1)$$

where $[acetone]_0$ is the initial concentration of acetone, $\{acetone^+\}_0$ is the corresponding measured counts, and $\Delta\{acetone^+\}$ is the difference between the counts of acetone ions before and after the laser fired. The concentrations of

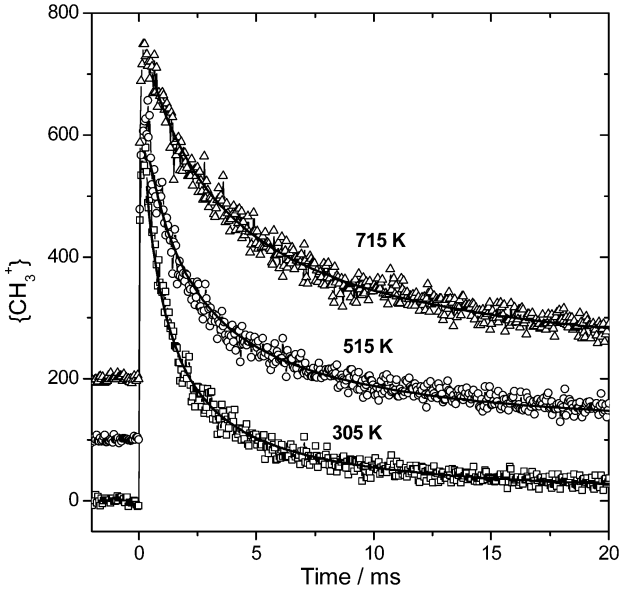

Figure 1. Experimental methyl ion signals ($m/e = 15$) vs time observed at 305 (□), 515 (○), and 715 K (△). For clarity, the profiles for 515 and 715 K were shifted upward by 100 and 200 counts, respectively. H_2-lamp photoionization. $P = 10$ Torr (He). $[CH_3]_0 = 1.1 \times 10^{13}$ cm^{-3}. The solid lines are the best-fit curves using eq E2.

methyl radicals were varied by changing the acetone concentrations in the range of $(0.1-65) \times 10^{13}$ molecules cm^{-3}.

Experimental Results and Discussion

The kinetic behavior of methyl radicals in this study is governed by the self-reaction R1 for two reasons: First, the heterogeneous loss rate of methyl radicals on the reactor wall, which was measured separately using low precursor concentrations, was very small (≤ 5 s^{-1}) at all temperatures and pressures considered here. Second, the concentration of CH_3 was always in large excess over all other radical concentrations. The most abundant secondary radical species were methylene radicals and hydrogen atoms. However, their initial concentrations were generally less than 2% of the methyl radical concentration. Under these conditions, the decay of CH_3 was largely unperturbed by secondary chemistry and, therefore, followed a simple second-order expression:

$$\frac{\{CH_3^+\}_t}{\{CH_3^+\}_0} = \frac{[CH_3]_t}{[CH_3]_0} = \frac{1}{2k_1[CH_3]_0 t + 1} \qquad \text{(E2)}$$

The observed methyl profile, denoted as $\{CH_3^+\}_t$, was fitted to the equation shown above with the reaction rate, $k_1' = k_1 \times [CH_3]_0$, and the initial counts, $\{CH_3^+\}_0$, as the fitting parameters. Finally, the rate constant k_1 was determined by a second-order plot of k_1' against $[CH_3]_0$. Experimental data of $\{CH_3^+\}_t$ taken in the interval between the laser pulse and 1 ms thereafter have been discarded in the fit. This treatment effectively eliminated two problems: First, the finite travel time from the orifice to the ionization region leads to a finite rise time in the methyl signal, which, however, was always negligibly short compared to the time scale of the observed kinetics. Second, vibrationally hot methyl radicals generated in the 193 nm photolysis of acetone were completely deactivated.[29]

Figure 1 shows typical profiles of methyl signal decays at different temperatures and 10 Torr He. As can be seen, the profiles could be fitted quite well using eq E2 in the time range of 1−20 ms. The best-fit reaction rates, $k_1' = k_1[CH_3]_0$, were then plotted against the concentrations $[CH_3]_0$, from which the rate constants k_1 could be obtained by linear least-squares fits (see Figure 2). The small values for the intercepts in the second-order plot are an indication that neither heterogeneous processes nor secondary reactions were important. The change of the rate constant was less than 5% if the fit was forced through the origin. Unfortunately, the precursor concentrations along the axis of the reactor were not uniform due to a pressure gradient caused by viscous flow through the small diameter tube. Therefore, the rate constants obtained from eq E2 were corrected according to the pressure drop, $\Delta P = P_{\text{entrance}} - P_{\text{exit}}$, which was measured in separate experiments:[30]

$$k_{1,\text{corr}} = k_1\left[1 + \frac{\Delta P}{2P_{\text{exit}}}\right]^{-1} \qquad \text{(E3)}$$

where the factor of 2 results from the fact that the orifice is located roughly in the middle of the reactor tube. The measured ΔP followed the theoretical expression for the pressure drop with ΔP (Torr) $= 5.9 \times 10^{-3} \upsilon \eta\, \Delta z/R^2$, where υ, Δz, and R are the flow velocity in cm/s, the distance in cm from the entrance, and the tube radius in cm, respectively. The pressure correction is temperature dependent by way of the bath gas specific viscosity, η (g cm^{-1} s^{-1}). Evidently, the pressure corrections tend to decrease the observed rate constant varying from 1% (10 Torr) to 16% (0.6 Torr) at 300 K for He bath gas. In total, twelve rate constants were obtained for He bath gas covering a pressure range of 0.6−10 Torr at three temperatures, (305 ± 5) K, (515 ± 25) K, and (715 ± 35) K (see Figure 3 and Table 1). For H_2 bath gas, room-temperature rate constants were measured at five pressures, i.e., 0.6, 1.1, 3.1, 6.1, and 10.1 Torr.

To establish error bounds incurred by neglecting secondary reactions, simulation calculations have been run on the following more detailed reaction mechanism:

$$CH_3 + CH_3 \rightarrow C_2H_6 \qquad \text{(R1)}$$

$$^3CH_2 + CH_3 \rightarrow C_2H_4 + H \qquad \text{(R4)}$$

$$CH_3 + H \rightarrow CH_4 \qquad \text{(R5)}$$

$$^3CH_2 + H \rightarrow CH + H_2 \qquad \text{(R6)}$$

$$^3CH_2 + {}^3CH_2 \rightarrow C_2H_2 + H_2 \qquad \text{(R7)}$$

Concentration profiles were calculated for two experimental conditions: $T = 300$ K, $P = 10$ Torr and $T = 700$ K, $P = 1.0$ Torr. The rate constants for R1 and R5 were set to be $k_1 = 6 \times 10^{-11}$ and $k_5 = 1 \times 10^{-11}$ cm^3 molecule^{-1} s^{-1} for the first case and $k_1 = 4 \times 10^{-12}$ and $k_5 = 1 \times 10^{-13}$ cm^3 molecule^{-1} s^{-1} for the second.[31] The rate constants of reactions R6 and R7 were chosen to be $k_6 = 2.2 \times 10^{-10}$ and $k_7 = 5.2 \times 10^{-11}$ cm^3 molecule^{-1} s^{-1}, for both temperatures and pressures.[32] A rate constant of $k_4 = 1.9 \times 10^{-10}$ cm^3 molecule^{-1} s^{-1} was used instead of 2.1×10^{-10} cm^3 molecule^{-1} s^{-1} reported by Wang and Fockenberg[27] because the original constant had been given without pressure correction. Two initial concentrations for CH_2 and H were chosen with $[CH_2]_0 = [H]_0$ and $[CH_2]_0/[CH_3]_0 = 1.5\%$ (the approximate experimental value) and 5% (to estimate an upper limit). The CH_3 profiles from the simulation were then fitted in the same way as outlined above giving rate constants, k_1^{sim}, which were then compared to the k_1 used. The difference between k_1 and k_1^{sim} changed from 0.3% to 5% at $T = 300$ K and $P = 10$ Torr and from 1% to 6% at $T = 700$ and $P = 1.0$

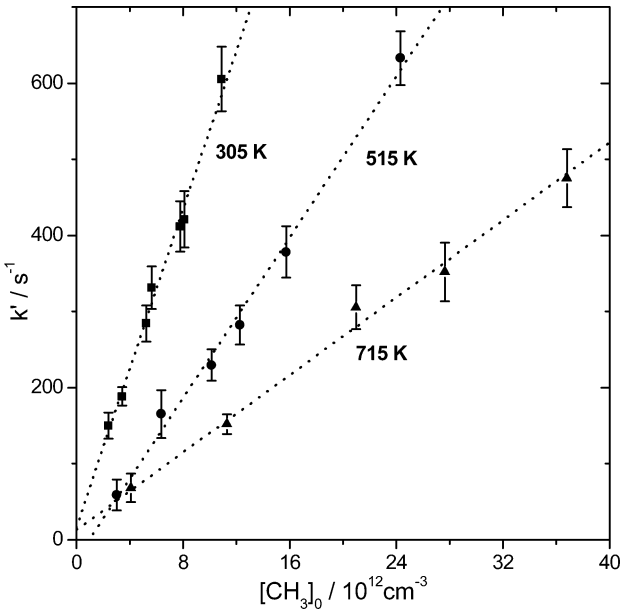

Figure 2. Second-order plots of the apparent reaction rates $k_1' = k_1[CH_3]_0$ vs $[CH_3]_0$ at the average temperatures 305 ± 5 (■), 515 ± 25 (●), and 715 ± 35 K (▲) at 10 Torr (He). The slopes obtained from the linear least-squares fits, shown as dashed lines, gave the rate constants, k_1: 5.27 ± 0.46, 2.64 ± 0.26, and 1.28 ± 0.14 in units of 10^{-11} cm^3 molecule^{-1} s^{-1} (± 2σ statistical errors).

Torr, as the concentration ratios $[CH_2]_0/[CH_3]_0$ and $[H]_0/[CH_3]_0$ were increased from 1.5% to 5%. This result supports the assumption that secondary reactions under the current experimental conditions have only marginal effects on the methyl kinetics.

As shown in Figure 3, the measured rate constants show a falloff behavior with negative temperature dependence. To compare our findings with rate constants found in the literature, we grouped the available data in temperature ranges of ±20 K around 300, 500, and 700 K. The open symbols in Figure 3 denote literature values for the rate constant k_1 in these temperature intervals with He bath gas. At room temperature, the data from this work are generally larger by as much as 40% than those obtained by Slagle et al.[2], Stoliarov et al.,[15] and Knyazev et al.[16] However, most recently, Knyazev et al.[17] reported $k_1 = (4.7 \pm 1.6) \times 10^{-11}$ cm^3 molecule^{-1} s^{-1} at $P =$ 3.7 Torr, which is very close to the value of $(4.81 \pm 0.52) \times 10^{-11}$ cm^3 molecule^{-1} s^{-1} at $P = 3.1$ Torr obtained here. Deters et al. reported a rate constant of $k_1 = 2.9 \times 10^{-11}$ cm^3 molecule^{-1} s^{-1} for 298 K and 1 Torr, which is about 30% smaller than our result.[18] Cody et al. published an even smaller value of 2.44×10^{-11} cm^3 molecule^{-1} s^{-1} measured under essentially the same experimental condition as mentioned above.[19] Interestingly, rate constants determined in experiments using flash photolysis with methyl radical concentrations measured from the drop of the precursor species tend to be faster than those where a microwave discharge is used to generate methyl radicals (F + $CH_4 \rightarrow CH_3$ + HF) in combination with titration methods to determine the concentration of the reactants.

In the study by De Avillez Pereira et al. the pressures employed at room temperature were larger than 7 Torr so that only rate constants, k_1, could be measured, which were near the high-pressure limit.[20] As mentioned before, the authors had to make corrections to their simple analysis due to interfering secondary reactions, which consisted mainly of contributions from the reaction of CH_3 radicals with H atoms. The corrected values found (4.8×10^{-11} cm^3 molecule^{-1} s^{-1} at 7.8 and 15 Torr) are consistent with rate constants obtained in this work (5.12×10^{-11} cm^3 molecule^{-1} s^{-1} at 6.1 Torr and 5.27×10^{-11} cm^3 molecule^{-1} s^{-1} at 10.1 Torr) in the regions of overlapping pressures in their experiments and ours.

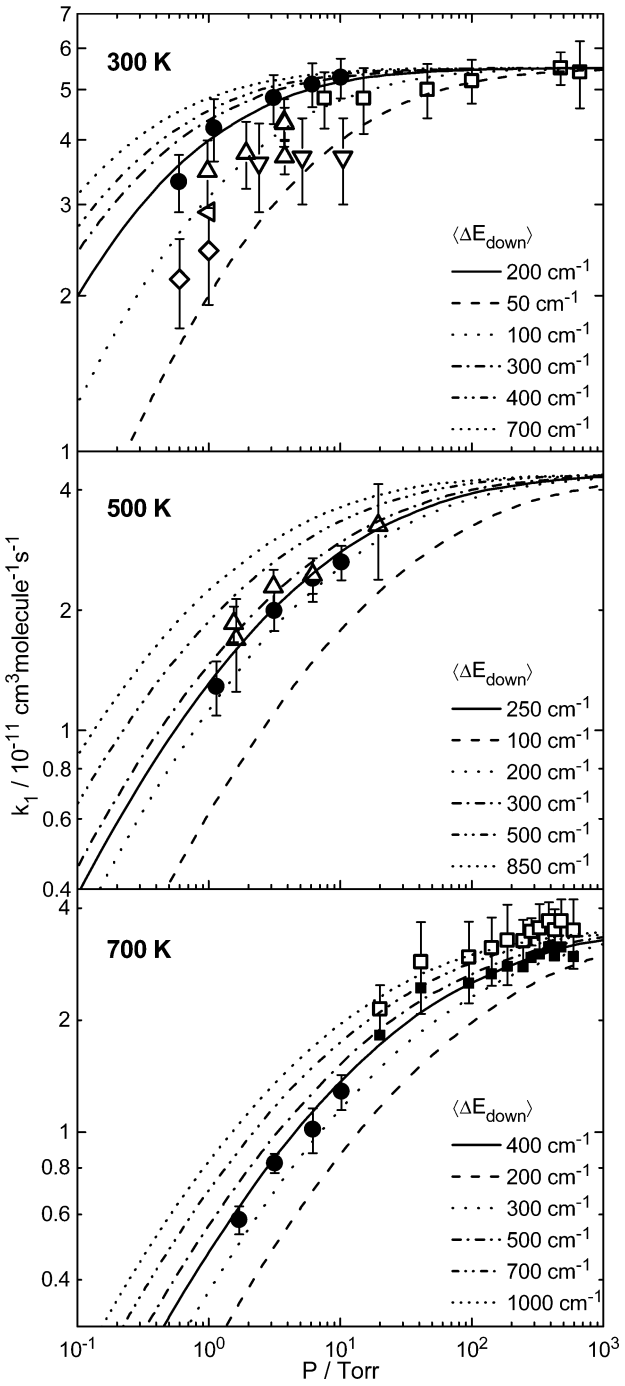

Figure 3. Pressure dependence of the theoretical and experimental rate constants of the $CH_3 + CH_3$ reaction for He as bath gas: ●, This work; ▽, ref 2; △, refs 15−17; (left-pointing triangle), ref 18; ◇, ref 19; □ and ×, ref 20. The filled squares (■) in the lower panel (700 K) show the data of ref 20 scaled by a factor of 0.85. As mentioned in the text, the temperatures shown are used to group experimental data measured at slightly different temperatures. The curves are the theoretical results calculated with various $\langle \Delta E_{down} \rangle$ values as indicated in the figures. The best fitting falloff curves to data of this work are marked as solid lines.

In contrast to the measurements at room temperature, at $T =$ 500 K, the data from this work are in good agreement with those obtained by Stoliarov et al.[15] At $T = 700$ K, our

TABLE 1: Measured Rate Constants for the Methyl−Methyl Recombination Reaction with He Bath Gas (k_1 in 10^{-11} cm^3 molecule^{-1} s^{-1}, 2σ Statistical Error)

$T = 305$ K		$T = 515$ K		$T = 715$ K	
P/Torr	k_1	P/Torr	k_1	P/Torr	k_1
0.6	3.32 ± 0.42	1.15	1.29 ± 0.20	1.7	0.58 ± 0.05
3.1	4.81 ± 0.52	3.15	1.99 ± 0.22	3.2	0.82 ± 0.05
6.1	5.12 ± 0.50	6.15	2.40 ± 0.30	6.2	1.02 ± 0.14
10.1	5.27 ± 0.46	10.15	2.64 ± 0.26	10.2	1.28 ± 0.14

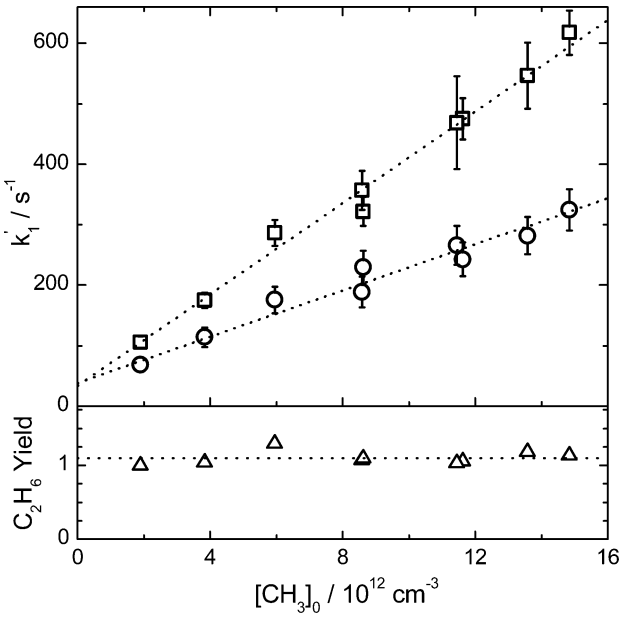

Figure 4. Methyl recombination rates $k_1' = k_1[CH_3]_0$ (upper panel) and the yield of ethane (lower panel), i.e., the ratio of $\{C_2H_6\}_\infty$ to the normalized drop of acetone in counts, $\Delta\{\text{acetone}^+\}96\%$ CR, with Ar as bath gas at 300 K. The linear least-squares fits, shown as dashed lines in the upper panel, gave the rate constants k_1(methyl) = 3.39 ± 0.36 from the decay of methyl radicals (□) and k_1(ethane) = 1.71 ± 0.24 from the ethane production (○) in units of 10^{-11} cm^3 molecule^{-1} s^{-1} (± 2σ statistical errors). The dashed line in the lower panel gave the average yield of ethane, 1.10 ± 0.13.

measurement of k_1 is the only one reported at pressures of P = 1.7−10.2 Torr. However, De Avillez Pereira et al. reported k_1 for higher pressures (200−594 Torr).[20] As can be seen in Figure 3, the uncorrected rate constants of De Avillez Pereira et al. indeed appear to be too high with respect to our low-pressure data. Unfortunately, the authors did not report corrected values for their high-temperature data. Therefore, we chose an average scaling factor of 0.85 for all rate constants in their 700 K data, which now appears to be a smooth continuation of our low-pressure data.

Although our high temperature and pressure rate constants compare favorably with earlier measurements by other groups, our low-pressure values measured at room temperature are consistently higher than literature data. Moreover, helium appears to be at least as effective as argon in deactivating the highly energized ethane complex. The most probable source of error in our measurements lies in the determination of the initial methyl radical concentration caused by systematic errors in experimental conditions (e.g., flow velocity, gas mixing ratio, pressure). Another source may be found in unidentified reactions of homogeneous or heterogeneous nature in the reactor. Correspondingly, two validations for our experiments were carried out. First, we attempted to reproduce the rate constant for the methyl recombination with Ar as bath gas, which has been well documented.[1−14] The room-temperature rate constant k_1 was

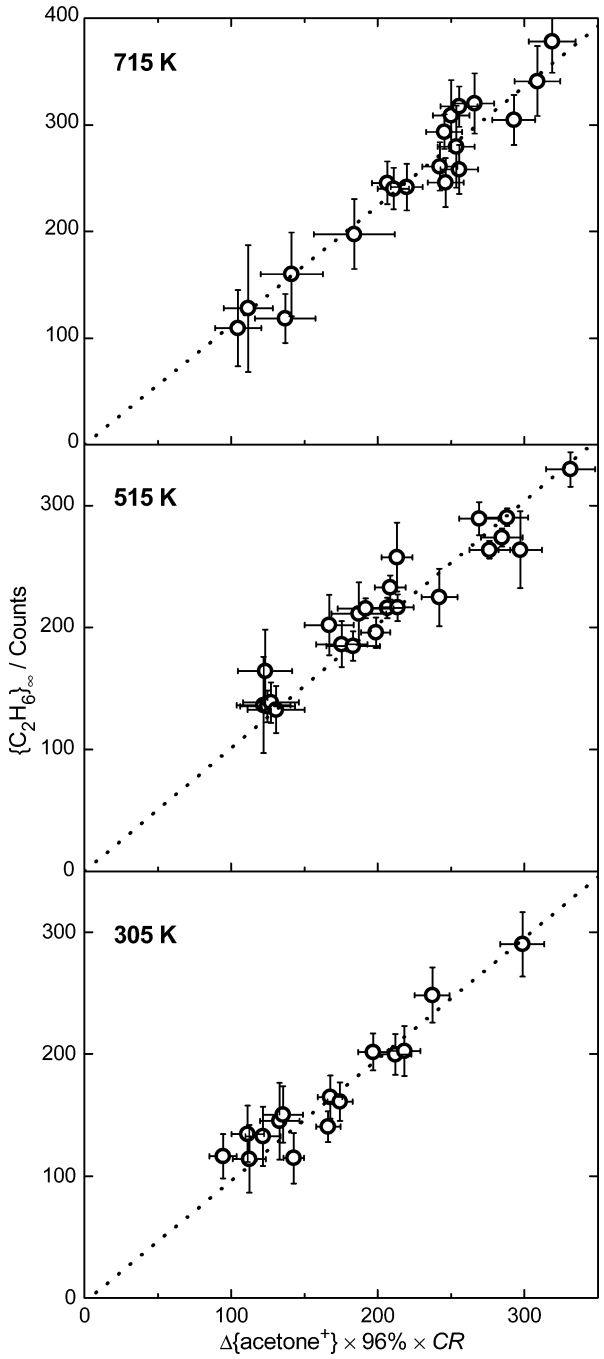

Figure 5. Extrapolated ethane yield in counts, $\{C_2H_6\}_\infty$, plotted versus the normalized drop of acetone in counts, $\Delta\{\text{acetone}^+\}96\%$ CR, at 305, 515, and 715 K. The dashed lines show the least-squares fits with the error bars as weights giving slopes of: 1.00 ± 0.17, 1.01 ± 0.09, and 1.16 ± 0.18 for 305, 515, and 715 K, respectively.

measured to be $(3.39 \pm 0.36) \times 10^{-11}$ cm^3 molecule^{-1} s^{-1} at P = 1.1 Torr of Ar (see Figure 4), which is in excellent agreement with the values of 3.51×10^{-11} cm^3 molecule^{-1} s^{-1} calculated from the global fit parameters evaluated by Hessler et al.[14] and $(3.3-4.0) \times 10^{-11}$ cm^3 molecule^{-1} s^{-1} measured at pressures between 0.75 and 1.5 Torr by Walter et al. using discharge flow mass spectrometry.[3] Second, the initial concentration of methyl radicals, $[CH_3]_0$, was validated by carbon balance analysis. Because all CH_3 radicals should be converted to the final product, C_2H_6, the ethane concentration at infinite time, $[C_2H_6]_\infty$, should be half of $[CH_3]_0$

$$[C_2H_6]_\infty = [CH_3]_0/2 = \Delta[\text{acetone}]96\% \qquad \text{(E4)}$$

This can be rewritten in terms of actual signal counts as

$$\{C_2H_6^+\}_\infty = \Delta\{\text{acetone}^+\}96\%\ \text{CR} \qquad \text{(E5)}$$

where CR is the calibration ratio of individual calibration constants for ethane and acetone concentrations measured in separate experiments. $\{C_2H_6^+\}_\infty$ was obtained by extrapolating the ethane profiles at $m/e = 30$ to infinite time using the following equation:

$$\frac{[C_2H_6]_t}{[C_2H_6]_\infty} = \frac{\{C_2H_6^+\}_t}{\{C_2H_6^+\}_\infty} = \frac{2k_1[CH_3]_0\, t}{2k_1[CH_3]_0\, t + 1} \qquad \text{(E6)}$$

For profiles with the reaction rates, $k_1[CH_3]_0$, larger than 300 s^{-1}, the conversion of methyl radicals to ethane was largely complete (≥90%) within the 15 ms time window of observation, giving a good estimate for $\{C_2H_6^+\}_\infty$. However, for smaller reaction rates, the reaction is too far from being complete; thus, the extrapolation of the ethane trace has to be considered carefully. In addition, lower methyl concentrations resulted in not only lower reaction rates but also lower signal-to-noise ratios in the ethane counts. Therefore, larger error bars, i.e., $\pm 10\sigma$ rather than $\pm 2\sigma$ statistical errors, have been quoted for these $\{C_2H_6^+\}_\infty$ values. All $\{C_2H_6^+\}_\infty$ data were plotted against the $\Delta\{\text{acetone}^+\}96\%$ CR data (see Figure 5). Linear least-squares fits were performed with the error bars as weights, giving slopes of 1.00 ± 0.17, 1.01 ± 0.12, and 1.16 ± 0.18 for 305, 515, and 715 K with intercepts close to zero. These results confirm that the initial concentration $[CH_3]_0$ was determined correctly via eq E1, and parallel reactions of methyl radicals with species other than a second methyl radicals could be ruled out.

In addition to the ethane yield, the reaction rate constant, k_1, could have been deduced from the rise of the ethane profiles as well. Unfortunately, the kinetics for the production of ethane are inconsistent with the decay of methyl radicals; that is, the rate constants obtained from the ethane production are persistently smaller than the rate constants determined from the methyl decay for all three bath gases: H_2, He, and Ar. The reason for this observation is not known. Interestingly, the relative difference between the two reaction rates observed, k_1' (C_2H_6) and k_1' (CH_3), vanishes with decreasing initial methyl concentrations, i.e., the slower the reaction proceeds the better the agreement is. Moreover, the discrepancy between the rate constants, $k_1 \times$ (CH_3) and k_1(C_2H_6), also diminishes with increasing pressure (see Figure 6). We suspect that this behavior is caused by a temporary loss of ethane signal at $m/e = 30$ due to increased fragmentation of energized ethane after ionization. As ethane is deactivated, it becomes "visible" again at its parent mass. In fact, we found evidence to support this idea by looking at masses $m/e = 26-29$ in separate experiments using a reaction tube with a larger orifice size to enhance the sensitivity of the apparatus. Signals at masses $m/e = 27$ and 29 show a fast rise and slower decay, which supports the proposed idea, which entails that the highest concentrations of excited ethane are found early in the reaction when the turnover rate is high as well (see Figure 7). In addition, the signal at mass $m/e = 28$ exhibits faster kinetics than the parent signal of ethane. However, a small contribution from ethylene to mass $m/e = 28$ produced in reaction R4 made it very difficult to analyze this signal quantitatively.

We also attempted to simulate the slower rise of the ethane signal by numerically integrating a simple reaction mechanism where C_2H_6* represents the final product still carrying some amount of internal energy:

$$CH_3 + CH_3 + M \rightarrow C_2H_6^* + M \qquad \text{(R1a)}$$

$$C_2H_6^* + M \rightarrow C_2H_6 + M \qquad \text{(R1b)}$$

$$^3CH_2 + CH_3 \rightarrow C_2H_4 + H \qquad \text{(R4)}$$

The relative fragmentation pattern of C_2H_6* was assumed to be the same as determined for Ne (16.67 and 16.85 eV) as discharge gas instead of H_2, giving an about three times higher yield for the ethylene ion fragment compared to the parent, ethane. Fitting rate constants for reactions R1a and R1b and allowing the fragmentation pattern to vary slightly we could capture the observed slower growth of the signal of the ethane parent ion. Rate constants for deactivating excited ethane were generally found to be around $k_{1b} \approx 10^{-13}$ cm^3 molecule^{-1} s^{-1}; that is, thermalization was completed in less than 1 ms depending on the bath gas pressure used, which does not seem to be excessively slow considering the fact that the initial internal energy of ethane produced in the recombination is about 4 eV. In addition, k_{1b} represents at best a cumulative collisional energy transfer rate. It has to be emphasized that it was not possible to extract any meaningful results from these data because the ionization efficiency and fragmentation pattern of excited ethane molecules is necessary information for a detailed analysis, which, however, are not known and their determination is beyond the scope of this experiment.

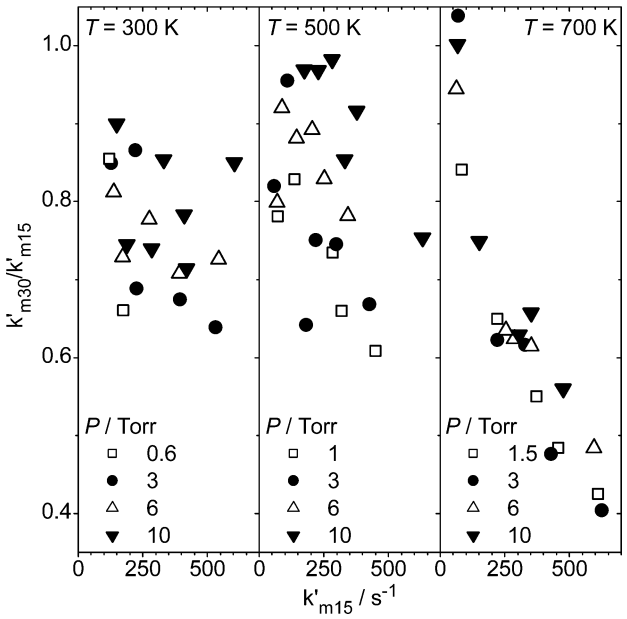

Figure 6. Ratios of the apparent reaction rate for the production of ethane (observed at $m/e = 30$) and the decay rate of the methyl radical concentration (k_{m30}/k_{m15}) versus the reaction rate of the methyl radicals (k_{m15}).

The overall yield should be unaffected by this behavior because at long times ($>(2 \times k_1[CH_3]_0)^{-1}$) the amount of excited ethane compared to already equilibrated ethane is small. Indeed, the ethane yield, i.e., the ethane produced per acetone photolyzed (see above), determined in the case of Ar as bath gas (1 Torr) can be given as 1.10 ± 0.13, despite the fact that the apparent rate of production was only half as fast as the decay of methyl radicals (see Figure 4).

Theoretical Calculations

Potential Energy Surface. For this work, we calculated two features of the potential energy surface that are important for

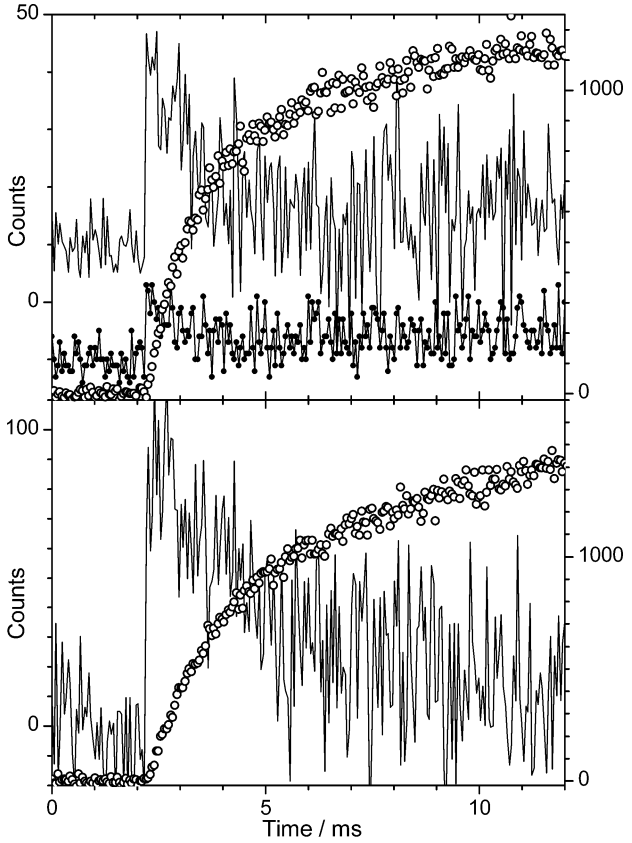

Figure 7. Signal trace of ethane at $m/e = 30$ (open circles, counts on right axes) as well as residual traces at $m/e = 27$ (line plus circle) and $m/e = 29$ (lines) after contributions due to fragmentation have been subtracted from the original signals. Upper panel: Ar discharge, $P =$ 1.1 Torr, $T = 510$ K, $[CH_3]_0 = 2.7 \times 10^{13}$ cm^{-3}; lower panel: H_2 discharge, $P = 1.1$ Torr, $T = 300$ K, $[CH_3]_0 = 4.8 \times 10^{12}$ cm^{-3}. The differences in the apparent rates obtained from the ethane rise relative to the methyl decay are 27% and 34%, respectively.

the kinetics of the methyl−methyl recombination reaction using the MOLPRO program suite.[33] The first feature is the long-range attractive interaction between the radical centers (carbon atoms) of two approaching methyl radicals (V_{CC}). The other one is the hindered internal rotation barrier between two CH_3 moieties ($V_{torsion}$). Both features have been calculated as a function of the C−C separation distance (R_{CC}).

Multireference configuration interaction (MRCI)[34] calculations were performed for V_{CC} employing orbitals from complete active space self-consistent field (CASSCF) wave functions with 14 valence electrons being distributed in eight active orbitals. In addition to the C−C bonding and antibonding orbitals, this active space includes the six CH bonding orbitals but not the corresponding six CH antibonding orbitals. Including the latter in CAS(14,14) reference functions would have made the subsequent MRCI calculations prohibitively laborious for carrying out geometry optimizations. Preliminary calculations indicated that the CAS(14,8) reference functions led to more reliable geometric properties than the CAS(2,2) reference functions obtained by omitting the CH bonding orbitals. Within the D_{3d} symmetry that corresponds to the staggered geometry of ethane, the structural parameters of the supermolecule, "$H_3C\cdot\cdot\cdot CH_3$," were fully optimized at fixed C−C distances using a DZP+diffuse basis set.[35] To minimize the error associated with the use of this relatively small basis set, the energies of the optimized structures were recalculated with larger basis sets, i.e., *aug*-cc-*p*VTZ for carbon atoms and cc-*p*VTZ for hydrogen atoms.[36] Moreover, a multireference Davidson correction (+Q)

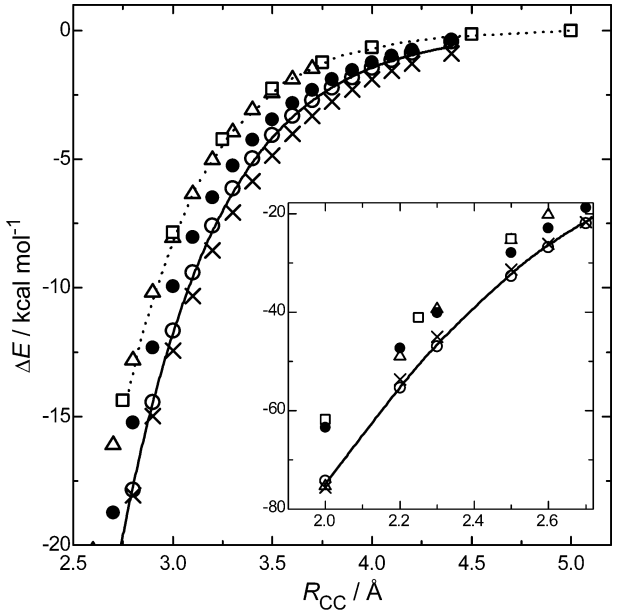

Figure 8. Relative energies, ΔE, calculated at the MRCISD+Q level as a function of the C−C distances, R_{CC}, for two approaching methyl fragments within D_{3d} symmetry (staggered orientation): ●, this work. The total energy of two methyl radicals at infinite separation distance was set to be zero. The solid line shows the least-squares fit to the scaled ab initio data (○, see text) using eq E7. The insert shows the ΔE values at shorter C−C distances (2.0−2.7 Å). ×, ref 9; △, ref 11; □, ref 13; - - -, ref 12.

was used to account for the effects of full CI.[37] Energies were computed for 22 C−C distances in the range of $2.0 \le R_{CC}$ (Å) ≤ 4.4 and are shown in Figure 8 (filled circles) as energy differences (ΔE) with respect to the total energy of two methyl radicals at infinite separation. The calculated data points were fitted to a Morse potential function

$$V_M = D_{CC}[1 - e^{-\beta_{CC}(R_{CC}-R_{e,CC})}]^2 - D_{CC} \qquad \text{(E7)}$$

where the parameters D_{CC} and $R_{e,CC}$ represent the dissociation energy and equilibrium C−C bond length, respectively. The parameter β_{CC} determines the steepness of the Morse potential. Because the MRCI+Q calculations underestimate the C−C bond dissociation energy, we scaled the Morse D_{CC} to agree with the experimental value. The scaled ab initio points are simply the calculated points multiplied by the ratio of the scaled and original Morse potentials at each distance. The parametric values for D_{CC}, $R_{e,CC}$, and β_{CC} are listed in Table 2.

Previous calculations for ΔE are also shown in Figure 8 for comparison. The data include the effective Morse potential by Wardlaw et al.[9] and Wagner et al.[10] (crosses), the empirical overlap integral potentials by Darvesh et al.[11] (triangles), the potential (dashed line) calculated by Klippenstein et al.[12] using MRCISD with the cc-pVDZ basis set, and the minimum energy reaction path (squares) calculated by Robertson et al.[13] using a generalized valence bond (GVB) theory with the 6-31G(d) basis set. For the calculated R_{CC} distances, the scaled ΔE values of this work are only slightly higher (by about 0.2−1 kcal/mol) than those of Wardlaw et al. and Wagner et al. but are significantly lower by as much as 6 kcal/mol at $R_{CC} = 2.7$ Å compared to calculations of Darvesh et al., Klippenstein et al., and Robertson et al. Because, according to the variational transition state calculations described below, the location of the transition state changes with temperature roughly from about 4.5 to 2.5 Å for $T = 200-1500$ K, a strong correlation between the recombination rate constant and ΔE is expected.

TABLE 2: Potential Parameters and Vibrational Frequencies Used for VARIFLEX Calculations[a]

		vibrational frequencies/cm^{-1} [b]			
		conserved modes		transitional modes	
potential parameters		2 CH_3 (ν_i^r)	C_2H_6 (ν_i^p)	2 CH_3	C_2H_6
D_{CC}	33877 cm^{-1} [c]				
D_{CH}	14.6 cm^{-1} [d]				
D_{HH}	6.0 cm^{-1} [d]	3004	2954	translation	995 (CC stretch)
$R_{e,CC}$	1.696 Å[e]	3004	2896	rotation	289 (torsion)
$R_{e,CH}$	3.625 Å[d]	606	1388	rotation	822 (CH_3 rock)
$R_{e,HH}$	3.370 Å[d]	606	1379	rotation	822 (CH_3 rock)
β_{CC}	2.1281 Å^{-1} [e]	3161	2985	rotation	1190 (CH_3 rock)
$\beta_{e,CH}$	2.2491 Å^{-1} [d]	3161	2985	rotation	1190 (CH_3 rock)
$\beta_{e,HH}$	2.4223 Å^{-1} [e]	3161	2969		
ϵ (C_2H_6)	234 cm^{-1} [f]	3161	2969		
ϵ (Ar)	114 cm^{-1} [f]	1402	1468		
ϵ (He)	10 cm^{-1} [f]	1402	1468		
ϵ (H_2)	60 cm^{-1} [f]	1402	1469		
σ (C_2H_6)	4.39 Å[f]	1402	1469		
σ (Ar)	3.47 Å[f]				
σ (He)	2.55 Å[f]				
σ (H_2)	2.83 Å[f]				

[a] The indices (C and H) denote interactions between pairs of atoms belonging to the different CH_3 reactants. [b] Reference 9. [c] Reference 46. [d] Reference 41. [e] This work. [f] Reference 43.

The barrier for the hindered internal rotation ($V_{torsion}$) of the ethane complex was calculated using the coupled-cluster theory with singles, doubles, and perturbative triple excitations, CCSD(T).[38] $V_{torsion}$ was determined to be the energy difference between the staggered geometry (D_{3d} symmetry) and the eclipsed geometry (D_{3h} symmetry) of the $H_3C\cdots CH_3$ system. With the C−C distance being fixed, the staggered (D_{3d}) geometry was optimized with the *aug*-cc-pVDZ basis set.[36] The corresponding eclipsed (D_{3h}) geometry was *defined* as that obtained by rotating one methyl group by 60° about the C−C bond of the optimized staggered geometry with all other geometric parameters of the staggered geometry frozen. The energies of both the staggered and eclipsed geometries were then calculated with two larger basis sets, i.e., *aug*-cc-pVTZ for carbon atoms and *aug*-cc-pVDZ for hydrogen atoms, and *aug*-cc-pVQZ for carbon atoms and *aug*-cc-pVDZ for hydrogen atoms.[36] The corresponding two energies were denoted as E_T and E_Q, respectively. The purpose of these two large-scale calculations is to extrapolate the CCSD(T) energies to the complete basis set (E_{CBS}) limit using the formulation suggested by Helgaker et al.[39]

$$E_{CBS} = \frac{64E_Q - 27E_T}{37} \tag{E8}$$

The final results of $V_{torsion} = E_{CBS}(\text{eclipsed}) - E_{CBS}(\text{staggered})$ are shown in Figure 9 (open circles). The torsion barrier decreases as the C−C distance increases. At $R_{CC} > 2.7$ Å, the torsion barrier is lower than 0.1 kcal/mol, implying an essentially free internal rotation of the two CH_3 moieties. Note that the present calculations of the torsional barrier extend no further than $R_{CC} = 2.7$ Å so that the well-known deficiencies of the CCSD(T) method at larger C−C distances were not encountered. The dashed line in Figure 9 was calculated from the potential surface of Wardlaw et al.,[9] which is a sum of the empirical pairwise Lennard-Jones potentials. The dotted line represents the results of Darvesh et al.,[11] who used the same expressions as those used here but with different parameters. Evidently the torsion potentials in both cases are significantly lower than ours, which is also reflected in the torsion barrier of ethane in its equilibrium geometry of 0.89 and 0.34 kcal/mol as calculated by Wardlaw et al. and Darvesh et al., respectively. In contrast, the theoretical value found here (2.84 kcal/mol) and that by Robertson et al.[13] (3.06 kcal/mol) compare favorably with the experimental value of 2.92 kcal/mol.[40] Although only a very small basis set, i.e., 6-31G(d), was used by Robertson et al. in the GVB calculation, the $V_{torsion}$ potential shown as triangles in Figure 9 is only slightly larger than our high-level data. However, as mentioned above, the C−C interaction potential calculated by Robertson et al. at the GVB level of theory is quite different from our high-level calculation.

For the transition state theory calculation, a global potential energy surface is needed. Analogous to the work of Wardlaw et al., an empirical analytic potential energy surface was built describing the interactions between two CH_3 radicals in the reaction entrance region. In brief, the potential energy was approximated as the sum of two terms. The first one is V_t for the transitional degrees of freedom, which are the vibrational degrees of freedom in the reaction product C_2H_6 arising from translational and rotational degrees of freedom of the two CH_3 radicals. The second one is V_c for the conserved vibrational degrees of freedom. Detailed definitions of the transitional and conserved vibrational modes and the corresponding vibrational frequencies have been listed in Table 2. For simplicity, V_c was assumed to be separable and quadratic. The potential V_t was set to be the sum of two terms: V_1 for the C−C interaction and V_2 for the C···H and H···H interactions between the two CH_3 fragments. V_1 is the same Morse potential as described in equation E7 but modified by two orientational factors[9]

$$V_1 = V_M \cos^2\theta_1 \cos^2\theta_2 \tag{E9}$$

where θ_1 and θ_2 are the angles between the C−C vector and the 3-fold symmetry axis of the two CH_3 radicals. V_2 is a sum of Morse-like potentials V_{ij}, as suggested by Darvesh et al.[11]

$$V_2 = \sum_{ij=\text{CH,HH}} V_{ij} \tag{E10}$$

$$V_{ij} = D_{ij} \times [1 - e^{-\beta_{ij}(R_{ij}-R_{e,ij})}]^2 - D_{ij} \tag{E11}$$

$$\beta_{ij} = \beta_{e,ij} + 0.01673(1 - R_{ij}/R_{e,ij}) \tag{E12}$$

where the indices *ij* represent the C···H and H···H pairs of the two CH_3 fragments. D_{ij} and R_{ij} are the corresponding potential well depths and separation distances. All parameters (D_{ij}, $R_{e,ij}$, and $\beta_{e,ij}$) were taken from the literature[9−11,41] except, $\beta_{e,HH}$, which was determined by fitting V_2 to the calculated torsion barriers. The parameters for eqs E7−E12 are listed in Table 2.

Transition State Theory Calculations. For the temperatures considered in this work, i.e., $200 \le T \le 1350$ K, the dominant reaction mechanism for the methyl−methyl recombination is the production of ethane on the singlet potential energy surface. The contribution from other product channels is negligible.[12] Using the variable reaction coordinate/flexible transition state theory, the dividing surface for the barrierless $CH_3 + CH_3$ reaction was found variationally at an E- (energy) and J- (total angular momentum) resolved level of theory. Then the effective bimolecular rate constants were calculated as a function of temperature and pressure by solving the one-dimensional master equation via a numerical matrix inversion algorithm. All theoretical calculations have been carried out using the VARIFLEX 1.0 program[42] with appropriate modifications.

An energy grain size of 50 cm^{-1} with the energies spanning the range from 8000 cm^{-1} below to 50 000 cm^{-1} above the threshold provides numerically converged results for the rate constants at all temperatures. Total angular momentum quantum

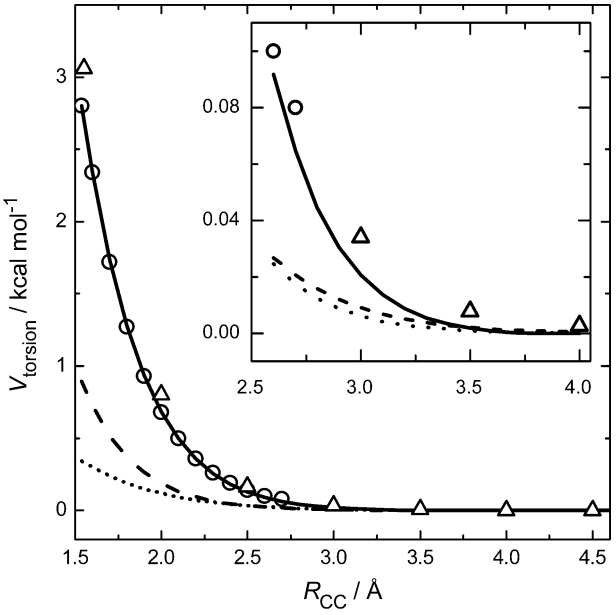

Figure 9. Torsion barriers calculated at the RCCSD(T) level versus the C−C separation distances. The insert shows an enlarged portion of the graph between 2.5 and 4.0 Å. The solid line shows the least-squares fit to the ab initio data of this work using eqs E10−E12. ○, This work; - - -, ref 9; ···, ref 11; △, ref 13.

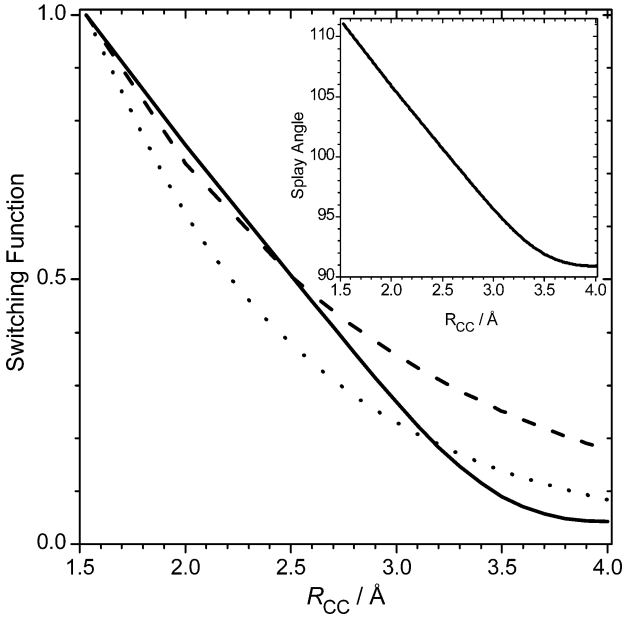

Figure 10. Switching function, f_s, (—) and CH_3-splay angle (inset) used in this work as a function of C−C distances, R_{CC}. The broken lines show the switching functions for an exponential dependence $f_s = e^{-\alpha(R-R_e)}$ with $\alpha = 1$ Å^{-1} (-·-) and $\alpha = 0.7$ Å^{-1} (- - -).

numbers ranging up to 150 were considered with a step size of 5. In the Monte Carlo integration 20 000 configurations were sampled with the convergence limit at about 5%.

A Lennard-Jones model was used to calculate the collision frequency between C_2H_6 and bath gases (Ar, He, and H_2) with the parameters σ (diameter) and ϵ (well depth) taken from Hippler et al. (see Table 2).[43] The energy transfer probability was evaluated using a simple exponential down model, which features only one downward energy transfer parameter, $\langle\Delta E_{down}\rangle$.[44] Because there are no experimental data for $\langle\Delta E_{down}\rangle$, a variety of values ranging from 50 to 1500 cm^{-1} have been examined in this work. Additionally, the biased random walk (BRW) model was used to provide an a priori estimate for $\langle\Delta E_{down}\rangle$.[44]

During recombination, the structure of the CH_3 group changes from a planar geometry to a splayed geometry along the reaction coordinate R. The vibrational frequencies for each geometry along the reaction coordinate were estimated by interpolation

$$\nu_i(R) = \nu_i^r + (\nu_i^p - \nu_i^r) f_s(R - R_e) \qquad \text{(E13)}$$

where R_e is the equilibrium value of R in C_2H_6 with the switching function, f_s, obtained from the calculated R dependence of the CH_3-splay angle along the minimum energy path (see Figure 10). More specifically, a smooth cubic spline fit through all of the calculated splay angles was shifted and scaled so that the resulting switching function has the values $f_s(\infty) = 0$ at large distances and $f_s(0) = 1$ at the equilibrium distance. The new switching function implies that the methyl−methyl recombination has a loose transition state at low temperatures, which tightens considerably at higher temperatures. In comparison, the exponential switching function $f_s = e^{-\alpha(R-R_e)}$ with $\alpha = 1.0$ Å^{-1} as used by Wardlaw and Marcus[9] suggests a transition state that is too loose at higher temperatures, whereas the transition state for $\alpha = 0.7$ Å^{-1} as used by Wagner and Wardlaw[10] is too tight except at the highest temperatures (see Figure 10). The reactant frequencies ν_i^r and the product frequencies ν_i^p are the conserved frequencies ($i = 1-12$) of two isolated methyl radicals and ethane, respectively, as defined in Table 2. The correlation of frequencies was taken from the work of Wardlaw and Marcus.[9] The torsion mode of the C_2H_6 was treated as a one-dimensional hindered internal rotor with a torsion barrier of 2.92 kcal/mol and a reduced rotational constant of 10.62 cm^{-1}.

TABLE 3: Optimized Reaction Path C−C Bond Distances from Iterative Canonical Calculations

T/K	*R*/Å	*T*/K	*R*/Å	*T*/K	*R*/Å	*T*/K	*R*/Å
200	7.06	407	3.77	577	3.56	810	3.35
290	4.00	473	3.69	600	3.55	900	3.28
296	3.95	500	3.67	715	3.42	1000	3.21
310	3.93	515	3.67	800	3.36	1350	2.97

The option "*R*-dependent geometries" in the VARIFLEX program was used to specify a methyl geometry at the transition state for each temperature. Because VARIFLEX 1.0 does not allow the geometry to adjust in the variational treatment, an "average" geometry for each temperature was found by carrying out thermally averaged (canonical) transition state calculations iteratively. Starting from planar methyl moieties at the transition state, a C−C distance, R_{CC}, was found at which the rate constant had a minimum. For the next run, the geometry for this particular R_{CC} was chosen resulting in a new optimized R_{CC}. After only three iterations, the calculations essentially converged giving optimized R_{CC} values for each temperature (see Table 3).

In addition, the VARIFLEX 1.0 program in its current form allows only fixed values for the symmetry number of the transition state. However, between the extreme boundaries, complete free rotation of the methyl moieties (planar CH_3) and the ethane product (pyramidal CH_3), the symmetry number changes from 72 to 18. Wardlaw and Marcus handled this problem by distinguishing planar and pyramidal geometries considered in their determination of the sum of states in the transition state and approximating a new sum of states according to the relative abundance of either geometry.[9] To accommodate this change in an empirical way here, the symmetry number instead of the sum of states for the transition state was adjusted using the same switching function mentioned above. For this, the original code had to be altered, replacing the original call

TABLE 4: Calculated High-Pressure Limit Rate Constants for the Methyl−Methyl Recombination Reaction (k_∞ in 10^{-11} cm^3 molecule^{-1} s^{-1})

T/K	k_∞	T/K	k_∞
200	6.30	700	3.57
296	5.55	906	3.11
300	5.50	1000	2.87
407	4.85	1350	2.55
500	4.38	2000	1.90
577	4.07		

for the symmetry number with a functional calculating the new symmetry number invoking the C−C bond distance used at that instance.

The pivot points were chosen to be the centers of mass of the methyl fragments. This provides a reasonable approximation to the dividing surface (transition state) because the separation distances between two reacting CH_3 fragments is always in the range of 2.5−4.5 Å for $T = 200-1500$ K.

Theoretical Results and Discussion

High-Pressure Limit Rate Constant. The high-pressure limit rate constant, k_∞, was calculated without any adjustable parameters. The theoretical results are listed in Table 4 and plotted in Figure 11 (solid line) along with experimental values for k_∞ at 200, 300, 407, and 473 K (symbols) taken from the literature,[1−3,20] for which we assumed that the rate constants measured at pressures larger than 100 Torr were in or at least very close to the respective high-pressure limit. The previous theoretical calculations by Cobos et al.,[8] Wagner et al.,[10] Darvesh et al.,[11] and Klippenstein et al.[12] have been included as well. It is evident that the theoretical rate constants from this work are in quite good agreement with the experimental data, underestimating the high-pressure limit rate constants by only 10%. A generalized three-parameter Arrhenius-expression was fit to the calculated high-pressure rate constant giving

$$k_\infty^{\text{theory}}(T) = 7.42 \times 10^{-11}\,(T/298\ \text{K})^{-0.69}\,\text{e}^{-88\ \text{K}/T}\ \text{cm}^3\ \text{molecule}^{-1}\ \text{s}^{-1} \quad \text{(E14)}$$

The fit deviates by less than ∼4% from the calculated k_∞^{theory} in the studied temperature range of $T = 200-1350$ K.

For comparison we calculated the high-pressure-limit rate constant with a constant symmetry number of 72 for the transition state for three temperatures: $k_\infty^{\sigma=72}$ (296 K) = 5.42 × 10^{-11} cm^3 molecule^{-1} s^{-1}; $k_\infty^{\sigma=72}$(500 K) = 4.21 × 10^{-11} cm^3 molecule^{-1} s^{-1}; $k_\infty^{\sigma=72}$ (1350 K) = 2.14 × 10^{-11} cm^3 molecule^{-1} s^{-1}. Not surprisingly, $k_\infty^{\sigma=72}$ is lower than those for which symmetry number switching was considered. However, the difference between the two models is only significant (>10%) for higher temperatures ($T >$ 1000 K) as the transition state is getting tighter. For these high temperatures, there are no experimental data for the high-pressure-limit available so that neither model can be verified at this point.

Wagner et al. calculated k_∞ using flexible transition state theory employing a semiempirical potential energy surface with one adjustable parameter.[10] This potential parameter was chosen so that the calculated k_∞ for 296 K is essentially the same as the measured rate constant reported by Hippler et al.[1] The results are shown in Figure 11 (dashed line). The agreement between theory and experiment is good at temperatures lower than 400 K. However, the calculated $k_\infty(T)$ displays a discontinuity at a temperature of about 500 K. The reason for this phenomenon is not clear.

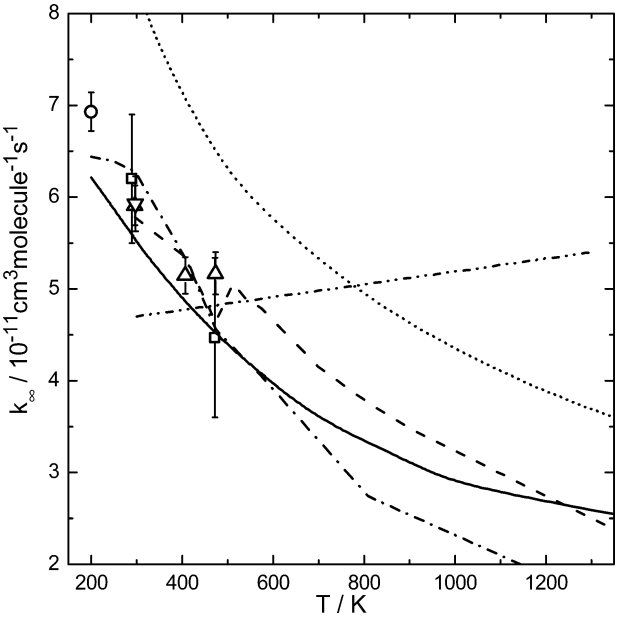

Figure 11. Plot of the temperature dependence of the theoretical high-pressure limit rate constant of the methyl−methyl recombination reaction. —, This work; -••-, ref 8; - - -, ref 10; •••, ref 11; -•-, ref 12. Experimental data: ▽, ref 1; △, ref 2; ○, ref 3; □, ref 20.

Compared to our calculations, the theoretical data for k_∞ obtained by Darvesh et al.[11] seem to have a qualitatively similar temperature dependence, however, shifted almost uniformly to higher rate constant values. The calculation method used by Darvesh et al. is very similar to the one used in this work but with two important differences in the potential energy surface: First, we used a Morse potential for the C−C interaction between two CH_3 radicals instead of an overlap-integral type of potential. Second, although we used the same atom−atom interaction potential functions, the potential parameters are different, especially for the hydrogen atom−atom interactions between two CH_3 radicals, resulting in their much lower torsion barrier than the value experimentally observed.

Klippenstein et al. carried out a direct transition state-theory-based study.[12] An arbitrary, temperature-dependent scaling factor had to be introduced by the authors with values ranging from 0.4 to 0.9 for $T = 407-1350$ K to match measured rate constants. The scaled results are shown in Figure 11 (dash-dotted line), which deviate only slightly at temperatures higher than 700 K compared to our calculated data.

In summary, it appears that the temperature dependence of k_∞ at temperatures between 200 and 500 K can be described well theoretically at the current level of theory. However, because of a lack of experimental data, predictions of k_∞ at higher temperatures seem less certain.

Pressure Dependence of the Rate Constant. The pressure-dependent rate constant was calculated with Ar bath gas first to check the performance against a large body of well-established experimental data. The results are shown in Figure 12. The experimental rate constants at $T = 200$ K were taken from the study of Walter et al.[3] All others were taken from the reevaluation of Hessler et al. and references therein.[14] As mentioned above, the energy transfer parameter, which describes the rate of deactivation of the excited C_2H_6* by collisions with bath gas molecules, was selected from a set of $\langle\Delta E_{\text{down}}\rangle$ values to explore the dependency of the deactivation efficiency on the shape of the falloff curve. The best energy transfer parameters from this set are shown in Figure 13.

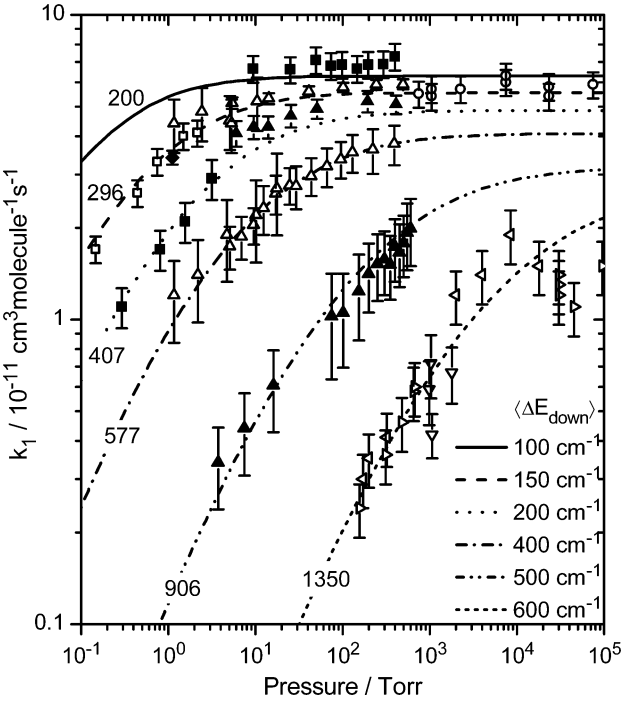

Figure 12. Plots of the pressure dependence of the rate constants, k_1, for Ar as bath gas at temperatures between 200 and 1350 K. ■ and □, ref 3; ○, ref 1; ▲ and △, ref 2; ▽, ref 7; (left-pointing triangle), ref 4; (right-pointing triangle), ref 5; ♦, this work. The lines are calculated falloff curves with energy transfer parameters, $\langle\Delta E_{down}\rangle$, as indicated in the plot.

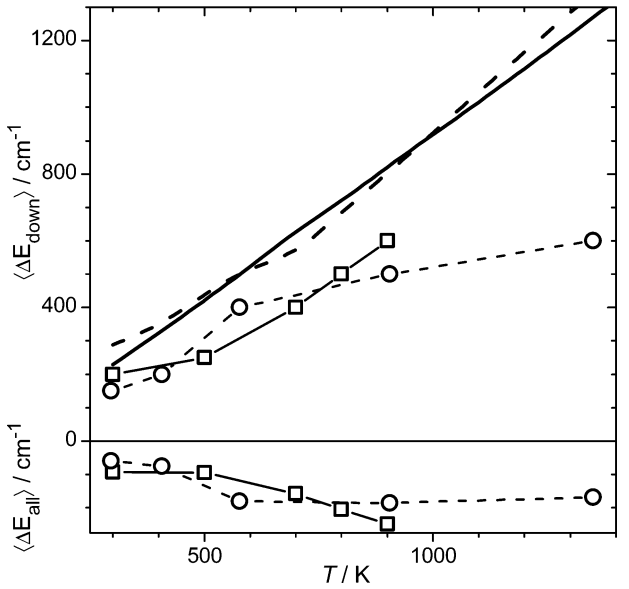

Figure 13. $\langle\Delta E_{down}\rangle$ and $\langle\Delta E_{all}\rangle$ values, for which the calculated falloff curves best fit the experimental data, versus temperature: for He (□) and Ar (○) as collision partners. The solid and dashed lines show the calculated $\langle\Delta E_{down}\rangle$ values using BRW model for He and Ar, respectively.

For the lowest temperature (200 K), experimental data are available only in the pressure range 9.5−441 Torr, in which the rate constants are very close to the high-pressure limit. Therefore, without any experimental rate constants at lower pressures, it is not possible to determine an approximate value for $\langle\Delta E_{down}\rangle$ to describe the falloff behavior at this temperature. For the C_2H_6−Ar collision, the BRW model gives $\langle\Delta E_{down}\rangle$ = 183 cm^{-1} at 200 K. According to the temperature dependence of the energy transfer parameters found here (Figure 13), $\langle\Delta E_{down}\rangle$ = 100 cm^{-1} appears to be a more appropriate value, for which the falloff curve was calculated (Figure 12) for future experimental validation.

At room temperature, the rate constant has been extensively measured using various experimental techniques in the pressure range covering 10^{-1}−10^5 Torr (Ar).[1−3] The falloff curve could be reproduced very well with $\langle\Delta E_{down}\rangle$ = 150 cm^{-1}. It is interesting to note that the BRW model predicted a higher value (270 cm^{-1}) for $\langle\Delta E_{down}\rangle$.

The experimental data between 407 and 906 K, which were taken mostly from the studies of Slagle et al.,[2] were also reproduced well theoretically with $\langle\Delta E_{down}\rangle$ values ranging from 200 to 500 cm^{-1}. Slagle's data for T = 906 K were scaled down according to Hessler et al.[14] based on lower UV absorption coefficients of methyl radicals than were originally used. It is worth noting that Wagner et al. calculated falloff curves for Ar as bath gas with an adjustable potential energy surface, as mentioned above.[10] A single energy transfer parameter, $\langle\Delta E_{all}\rangle$, which is the total average energy change in the metastable C_2H_6* per collision with bath gas molecules, was optimized by the minimization of the weighted root-mean-square of the relative error between theory and experiment. A value of $\langle\Delta E_{all}\rangle = -205 \pm 65$ cm^{-1} could reproduce the experimental data reported by Slagle et al. covering T = 296−906 K. Our calculations indicate a slight temperature dependence of this parameter; however, the average value $\langle\Delta E_{all}\rangle_{avg} = -134$ cm^{-1} is close to the one published by Wagner et al.

At T = 1350 K, the rate constants were measured by four groups.[4−7] Although the experimental data are fairly scattered above 1000 Torr, the calculated rate constants fit the whole body of data with $\langle\Delta E_{down}\rangle$ = 600 cm^{-1}. At such a high temperature, the high-pressure limit cannot be reached until the Ar bath gas pressure increases to around 10^7 Torr.

Because the theoretical calculations of the rate constants with Ar bath gas were successful, similar calculations have been carried out for He bath gas. The experimental rate constants k_1 along with the calculated falloff curves for different $\langle\Delta E_{down}\rangle$ values are shown in Figure 3. It can be seen that at room temperature the calculated falloff curve with $\langle\Delta E_{down}\rangle$ = 200 cm^{-1} represents the experimental data from this work at low pressures and the data of De Avillez Pereira et al. at high pressures very well.[20] A lower value of $\langle\Delta E_{down}\rangle$ = 50−100 cm^{-1} was needed to accommodate the lower rate constants obtained at 1 Torr reported by Slagle et al.,[2] Deters et al.,[18] and Cody et al.[19] At 500 and 700 K, the calculated falloff curves with $\langle\Delta E_{down}\rangle$ = 250 and 400 cm^{-1}, respectively, agree well with the corresponding experimental rate constants obtained here.

Figure 13 illustrates the $\langle\Delta E_{down}\rangle$ values used in this work for both He and Ar bath gases. It is evident that $\langle\Delta E_{down}\rangle$ exhibits a moderate positive temperature dependence. For the temperature range covered here, $\langle\Delta E_{down}\rangle$ values for He are similar to the ones for Ar, which is qualitatively supported by the BRW model. Quantitatively, the BRW model predicts $\langle\Delta E_{down}\rangle$ values which are roughly 30% larger than what was observed here; that is, the BRW model appears to be reliable for estimating the energy transfer parameter at moderate temperatures.[44]

Unfortunately, an unambiguous energy transfer parameter cannot be assigned to the experimental rate constants for H_2 bath gas measured at room temperature. The obtained rate constants as well as calculated falloff curves are shown in Figure 14. However, the data suggest that $\langle\Delta E_{down}\rangle$ is larger than 300 cm^{-1}, which makes hydrogen a more efficient quencher than

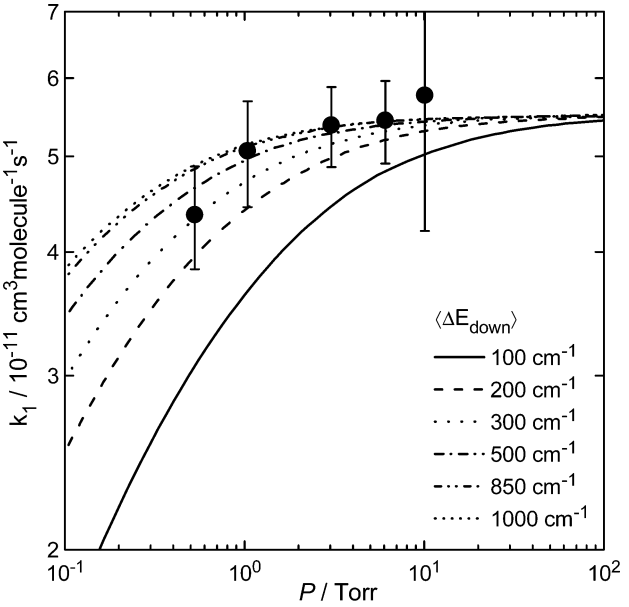

Figure 14. Plots of the pressure dependence of the rate constant with H_2 as bath gas at room temperature. The circles denote the experimental rate constants (after pressure correction) measured here. The lines denote the calculated falloff curves with $\langle\Delta E_{down}\rangle$ values as indicated in the figure.

He or Ar. This is in disagreement with the BRW model, which predicts a smaller value of $\langle\Delta E_{down}\rangle = 130$ cm^{-1}.

Global Fit. Global fits provide useful descriptions for the rate constants as a function of temperature and pressure with a moderate number of parameters. For this purpose, many empirical formulas are available in the literature. Troe's equation has been widely used in this respect[45]

$$k(T,P) = \frac{k_\infty P_r}{1+P_r} \times (F_{cent})^X \qquad \text{(E15)}$$

$$P_r = \frac{k_0}{k_\infty} \times \frac{P}{RT} \qquad \text{(E16)}$$

$$X = \left[1 + \left(\frac{lgP_r + c}{N - d(lgP_r + c)}\right)^2\right]^{-1} \qquad \text{(E17)}$$

where $c = -0.4-0.67\ lg(F_{cent})$, $N = 0.75-1.27\ lg(F_{cent})$, $d = 0.14$. R is the gas constant. Instead of fitting the high-pressure limit rate constant, k_∞, the Arrhenius expression of $k_\infty^{theory}(T)$ (eq E14) was used as is. The temperature dependence of the centering parameter is usually given as a four-parameter equation

$$F_{cent}(T) = (1-a)e^{-T/T^{***}} + ae^{-T/T^{*}} + e^{-T^{**}/T} \qquad \text{(E18)}$$

The least-squares fitting routine tended to set the parameter "a" to zero and the parameter T^{**} to infinity in a very shallow minimum so that the last two terms were neglected for the final analysis. The global fit was performed for 74 rate constants for He bath gas consisting of experimental data covering 202−900 K and 0.6−678 Torr reported by Cody et al.,[19] Slagle et al. (577 and 810 K),[2] Stoliarov et al.,[15] Knyazev et al.,[16,17] De Avillez Pereira et al.,[20] and this work. As mentioned above, the data of De Avillez Pereira et al. at $T = 473$ and 700 K were scaled by a common factor of 0.85. A Levenberg−Marquardt

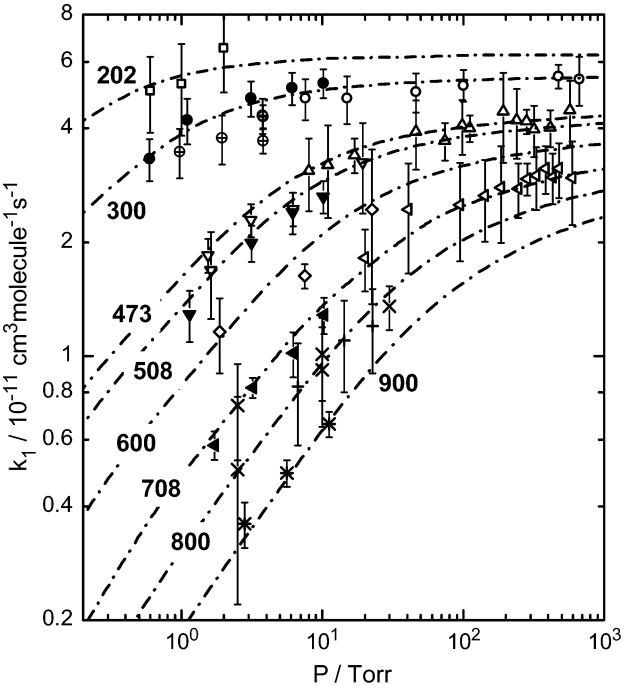

Figure 15. Plots of the pressure dependence of the rate constants, k_1, for He as bath gas at 202 K: □, ref 19. 290 K: ○, ref 20. 305 K (average temperature): ●, this work; ⊕, refs 15−17. 473 K: △, ref 20. 500 K: ▽, refs 16 and 17. 515 K: ▼, this work. 600 K: ◇, refs 16 and 17. 700 K: (left-pointing open triangle), ref 20. 715 K: (left-pointing solid triangle), this work. 800 K: ×, refs 16 and 17. 810 K: +, ref 2. 900 K: *, ref 15. The dashed lines are results of a global fit of Troe's equation (E15−E18) to the data points shown. The falloff curves were plotted for the temperatures as indicated in the plot.

nonlinear least-squares fit gives the following results: (see Figure 15)

$$k_0(T) = 1.17 \times 10^{-25}(T/298\ \text{K})^{-3.75}\ e^{-494\ \text{K}/T}\ \text{cm}^6\ \text{molecule}^{-2}\ \text{s}^{-1}$$
$$a = 0, \quad T^{***} = 570\ \text{K} \qquad \text{(E19)}$$

Conclusions

In this paper, we reported experimental measurements of the rate constant for the methyl−methyl recombination reaction as a function of temperature (305, 515, and 715 K) and pressure (0.6−10 Torr). He, H_2, and Ar were used as bath gases. The measured rate constants show negative temperature dependence and typical falloff behavior.

A new potential energy surface was developed for TST calculations. Without any adjustable parameters, the calculated high-pressure-limit rate constants are in very good agreement with the available experimental data. Moreover, the whole body of experimental rate constants with Ar and He bath gases could be well reproduced theoretically by solving the master equation with only one adjustable parameter $\langle\Delta E_{down}\rangle$ for the collisional energy transfer between the reaction product, ethane, and the three bath gases. The $\langle\Delta E_{down}\rangle$ values were shown to have a positive temperature dependence for both He and Ar. The current theoretical calculations suggest that He and H_2 as collision partners are as effective as Ar in deactivating highly energized ethane molecules. Unfortunately, there are no experimental data for the high-pressure limit rate constant at elevated temperatures (>500 K), which could help to calibrate future calculations and make predictions of the temperature dependence of k_∞ more reliable.

Acknowledgment. This work was performed at Brookhaven National Laboratory under Contract DE-AC02-98CH10886 with the U.S. Department of Energy and supported by its Division of Chemical Sciences, Office of Basic Energy Sciences.

References and Notes

(1) Hippler, H.; Luther, K.; Ravishankara, A. R.; Troe, J. *Z. Phys. Chem. NF* **1984**, *142*, 1.
(2) Slagle, I. R.; Gutman, D.; Davies, J. W.; Pilling, M. J. *J. Phys. Chem.* **1988**, *92*, 2455.
(3) Walter, D.; Grotheer, H.-H.; Davies, J. W.; Pilling, M. J.; Wagner, A. F. Experimental and Theoretical Study of the Recombination Reaction $CH_3 + CH_3 = C_2H_6$. Twenty-Third Symposium (International) on Combustion; University of Orleans, France, 1990.
(4) Glänzer, K.; Quack, M.; Troe, J. CH_3 recombination rate constants at high T & P; Sixteenth Symposium (International) on Combustion; The Combustion Institute: Seattle, WA, 1977.
(5) Hwang, S. M.; Rabinowitz, M. J.; Gardiner, J.; William C. *Chem. Phys. Lett.* **1993**, *205*, 157.
(6) Davidson, D. F.; Dirosa, M. D.; Chang, E. J.; Hanson, R. K.; Bowman, C. T. *Int. J. Chem. Kinet.* **1995**, *27*, 1179.
(7) Du, H.; Hessler, J. P.; Ogren, P. J. *J. Phys. Chem.* **1996**, *100*, 974.
(8) Cobos, C. J.; Troe, J. *J. Chem. Phys.* **1985**, *83*, 1010.
(9) Wardlaw, D. M.; Marcus, R. A. *J. Phys. Chem.* **1986**, *90*, 5383.
(10) Wagner, A. F.; Wardlaw, D. M. *J. Phys. Chem.* **1988**, *92*, 2462.
(11) Darvesh, K. V.; Boyd, R. J.; Pacey, P. D. *J. Phys. Chem.* **1989**, *93*, 4772.
(12) Klippenstein, S. J.; Harding, L. B. *J. Phys. Chem. A* **1999**, *103*, 9388.
(13) Robertson, S. H.; Wardlaw, D. M.; Hirst, D. M. *J. Chem. Phys.* **1993**, *99*, 7748.
(14) Hessler, J., P.; Ogren, P. J. *J. Phys. Chem. A* **1996**, *100*, 984.
(15) Stoliarov, S. I.; Knyazev, V. D.; Slagle, I. R. *J. Phys. Chem. A* **2000**, *104*, 9687.
(16) Knyazev, V. D.; Slagle, I. R. *J. Phys. Chem. A* **2001**, *105*, 3196.
(17) Knyazev, V. D.; Slagle, I. R. *J. Phys. Chem. A* **2001**, *105*, 6490.
(18) Deters, R.; Otting, M.; Wagner, H. G.; Temps, F.; Dóbé, S. *Ber. Bunsen-Ges. Phys. Chem.* **1998**, *102*, 978.
(19) Cody, R. J.; Payne, W. A., Jr.; Thorn, R. P., Jr.; Nesbitt, F. L.; Iannone, M. A.; Tardy, D. C.; Stief, L. J. *J. Phys. Chem. A* **2002**, *106*, 6060.
(20) Pereira, R. D. A.; Baulch, D. L.; Pilling, M. J.; Robertson, S. H.; Zeng, G. *J. Phys. Chem. A* **1997**, *101*, 9681.
(21) Fahr, A.; Laufer, A. H.; Klein, R.; Braun, W. *J. Phys. Chem.* **1991**, *95*, 3218.
(22) Oref, I. *J. Phys. Chem.* **1989**, *93*, 3465.
(23) Oref, I.; Tardy, D. C. *Chem. Rev.* **1990**, *90*, 1407.
(24) Wardlaw, D. M.; Marcus, R. A. *Chem. Phys. Lett.* **1984**, *11*, 230.
(25) Wardlaw, D. M.; Marcus, R. A. *J. Chem. Phys.* **1985**, *83*, 3462.
(26) Fockenberg, C.; Bernstein, H. J.; Hall, G. E.; Muckerman, J. T.; Preses, J. M.; Sears, T. J.; Weston, R. E., Jr. *Rev. Sci. Instr.* **1999**, *70*, 3259.
(27) Wang, B.; Fockenberg, C. *J. Phys. Chem. A* **2001**, *105*, 8449.
(28) Lightfoot, P. D.; Kirwan, S. P.; Pilling, M. J. *J. Phys. Chem.* **1988**, *92*, 4938.
(29) Donaldson, D. J.; Leone, S. R. *J. Phys. Chem.* **1987**, *91*, 3128.
(30) Howard, C. *J. Phys. Chem.* **1979**, *83*, 3.
(31) Marinov, N. M. *Int. J. Chem. Kinet.* **1999**, *31*, 183.
(32) Baulch, D. L.; Cobos, C. J.; Cox, R. A.; Esser, C.; Frank, P.; Just, T.; Kerr, J. A.; Pilling, M. J.; Troe, J.; Walker, R. W.; Warnatz, J. *J. Phys. Chem. Ref. Data* **1992**, *21*, 411.
(33) MOLPRO is a package of ab initio programs written by Werner, H.-J.; Knowles, P. J. with contributions from R. D. Amos, A. Bernhardsson, A. Berning, P. Celani, D. L. Cooper, M. J. O. Deegan, A. J. Dobbyn, F. Eckert, C. Hampel, G. Hetzer, T. Korona, R. Lindh, A. W. Lloyd, S. J. McNikolas, F. R. Manby, W. Meyer, M. E. Mura, A. Nicklass, P. Palmieri, R. Pitzer, G. Rauhut, M. Schutz, H. Stoll, A. J. Stone, R. Tarroni, and T. Thorsteinsson.
(34) Werner, H.-J.; Knowles, P. J. *J. Chem. Phys.* **1988**, *89*, 5803.
(35) Dunning, T. H., Jr.; Hay, P. J. DZP basis set. In *Methods of Electronic Structure Theory*; Schaefer, H. F., III., Ed.; Plenum Press: New York, 1977; Vol. 2.
(36) Dunning, T. H., Jr. *J. Chem. Phys.* **1989**, *90*, 1007.
(37) Langhoff, S. R.; Davidson, E. R. *Int. J. Quantum Chem.* **1974**, *8*, 61.
(38) Purvis, G. D.; Bartlett, R. J. *J. Chem. Phys.* **1982**, *76*, 1910.
(39) Helgaker, T.; Klopper, W.; Koch, H.; Nagel, J. *J. Chem. Phys.* **1997**, *106*, 9639.
(40) Weiss, S.; Leroi, G. E. *J. Chem. Phys.* **1968**, *48*, 962.
(41) Allen, M. P.; Tildesley, D. J. *Computer Simulation of Liquids*; Clarenden Press: Oxford, U.K., 1987.
(42) Klippenstein, S. J.; Wagner, A. F.; Dunbar, R. C.; Wardlaw, D. M.; Robertson, S. H. VARIFLEX; 1.0 ed.; Argonne National Laboratory: Argonne, IL, 1999.
(43) Hippler, H.; Troe, J.; Wendelken, H. J. *J. Chem. Phys.* **1983**, *78*, 6709.
(44) Gilbert, R. G.; Smith, S. C. *Theory of Unimolecular Recombination Reactions*; Blackwell Scientific: Oxford, U.K., 1990.
(45) Gilbert, R. G.; Luther, K.; Troe, J. *Ber. Bunsen-Ges. Phys. Chem.* **1983**, *87*, 169.
(46) Wagman, D. D.; Evans, W. H.; Parker, V. B.; Schumm, R. H.; Halow, I.; Bauley, S. M.; Churney, K. L.; Nuttall, R. L. *J. Phys. Chem. Ref. Data* **1982**, *11*, Suppl. 2.